Fluorescent liquid-core/air-cladding waveguides towards integrated optofluidic light sources†

Jong-Min Lim, Se-Heon Kim, Jae-Hoon Choi and Seung-Man Yang*

Received 31st March 2008, Accepted 4th June 2008
First published as an Advance Article on the web 18th July 2008
DOI: 10.1039/b805341c

We have demonstrated fluorescent liquid-core/air-cladding (LA) waveguides suitable for use as integrated optofluidic light sources. These waveguides were fabricated by conventional soft lithography using poly(dimethylsiloxane) (PDMS). Two-phase stratified flows of air and ethylene glycol with fluorescent dye were generated along the PDMS channel. Compared to the liquid-core/liquid-cladding (L^2) waveguide, the larger refractive index contrast of the LA waveguide resulted in stronger optical confinement. Specifically, the larger refractive index contrast led to experimentally achievable captured fractions (the amount of light to be coupled into the liquid core) as high as 22.8% and the measured propagation losses as low as 0.14 dB cm^{-1}. Furthermore, in our LA waveguides, diffusional mixing of the core and cladding fluids did not occur and the size of the core stream could be reversibly tuned simply by adjusting the flow rates of the two contiguous phases.

1. Introduction

Light sources and waveguides are essential building blocks in the emerging field of optofluidics, which combines optics and microfluidics.[1,2] Over the years, considerable effort has been devoted to devising new waveguide designs that are compatible with liquids. A few examples are Teflon-based waveguides,[3–5] silicon-based hollow waveguides,[6] nanoporous waveguides,[7] antiresonant reflecting optical waveguides,[8–12] waveguides based on photonic bandgap properties,[13–16] glass waveguides directly fabricated by femtosecond laser,[17] and others.[18,19] Recently, waveguides made of PDMS[20–28] have received special attention because they are inexpensive, amenable to rapid prototyping, and free from manual alignment. In particular, Backhouse's group demonstrated the optical waveguide integrated fluorescence detection devices.[27,28] However, the waveguide has large propagation loss (≈1.0 dB cm^{-1}), which is sensitive to the surface roughness of waveguide walls.

On the other hands, the fluorescent liquid-core/liquid-cladding (L^2) waveguides developed by Whitesides' group have optically smooth side walls and a wide range of tunability.[22–24] When the fluorescent dye molecules are pumped, a certain fraction of the isotropically emitted light can be captured and guided by total internal reflection. However, the small refractive index contrast ($\Delta n \approx 0.1$) between the liquid-core and the liquid-cladding reduces the amount of light captured in the core out of the isotropic fluorescent emission. Moreover, although L^2 waveguides function in the laminar flow regime, diffusional mixing of the core and cladding liquids can reduce the refractive index contrast in the downstream region of the microfluidic channel.[23]

In the present study, we developed a new type of waveguide in which air is used as the cladding layer with the aim of overcoming some of the major drawbacks of the L^2 waveguide without losing its unique advantages. Our fluorescent liquid-core/air-cladding (LA) waveguide adopts two-phase stratified flows of dye-containing ethylene glycol and air. The stream of fluorescent dye-containing ethylene glycol ($n_{EG} = 1.432$) that acts as a core is introduced using a syringe pump with a controlled flow rate, while the flow of air ($n_{air} = 1.000$) that acts as a cladding layer is induced by vacuum suction.[29,30] The size of the core stream can be tuned reversibly by changing the flow rate of ethylene glycol or the air suction pressure. The larger refractive index contrast between the liquid core and air cladding ($\Delta n = 0.432$) compared to the contrast between the liquid-core and liquid-cladding in the L^2 waveguide means that the LA waveguide can capture a larger fraction of the emitted light than the L^2 waveguide. LA waveguides are also free from diffusional mixing of the core and cladding fluids. In addition, the fluorescent LA waveguide is suitable for use as a portable integrated light source for micro-total analysis systems (micro-TAS), because the air used as the sheath fluid can be readily obtained from the environment.[29] Also, the fluorescent LA waveguide can be integrated as an internal light source into optofluidic devices with precise alignment.

2. Experimental

2.1 Fabrication of microfluidic chips

Fig. 1 shows schematic top views of PDMS devices for two different types of LA waveguides. The fluorescent LA waveguide shown in Fig. 1a was used for characterization of propagation

National Creative Research Initiative Center for Integrated Optofluidic Systems and Department of Chemical and Biomolecular Engineering, KAIST, Daejeon, 305-701, Korea. E-mail: smyang@kaist.ac.kr; Fax: +82-42-869-5962; Tel: +82-42-869-3922

† Electronic supplementary information (ESI) available: Monte Carlo simulation of the captured fractions. See DOI: 10.1039/b805341c

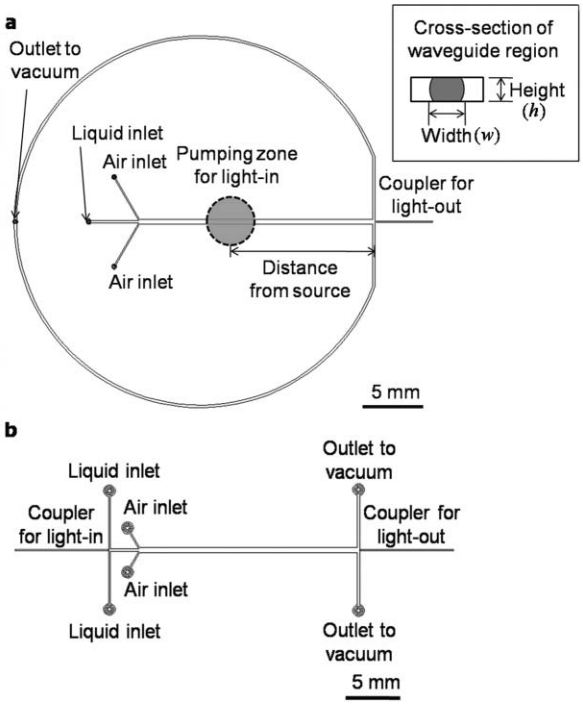

Fig. 1 Schematic top-view of the PDMS microfluidic devices for (a) the fluorescent LA waveguide and (b) the fiber-to-LA waveguide-to-fiber. The inset shows a schematic cross-sectional view of the LA waveguide.

losses due to the ease with which we can change the separation distance between the pumping spot and the 'T' intersection in this system. Since the guided fluorescent light from the source couples to the optical fiber at the 'T' intersection, the distance from the source can be viewed as the optical path length, as shown in Fig. 1a. The PDMS microfluidic device for the fiber-to-LA waveguide-to-fiber shown in Fig. 1b was used for calculating the total coupling loss by coupling a known amount of optical power from the laser diode. The coupling losses associated with both the optical fiber-to-waveguide and waveguide-to-optical fiber were included in the total coupling loss. The inset of Fig. 1 shows schematic cross-sectional views of the waveguides. In both waveguides, the width of the microfluidic channel for two-phase stratified flow is 400 μm and the width of the empty space acting as a pre-aligned coupler for optical fiber insertion is 126 μm.

Conventional photolithography using a negative photoresist (SU-8 100, MicroChem) and a soft-lithographic procedure using PDMS were employed to prepare the microfluidic channels. The negative photoresist was patterned using the method specified by the manufacturer, with slight modification to optimize the thickness and sharpness of the master. First, a 140 μm-thick uniform film of negative photoresist was coated on a silicon wafer by spin coating at 1500 rpm for 65 s. Then, to evaporate the solvent, the spin-coated negative photoresist was sequentially baked on hotplates (RET control-visc, IKA) at two different temperatures of 65 °C and 95 °C. The hotplates used for soft baking should be exactly level to ensure that the photoresist film remains uniform. The photoresist film was then exposed to UV light (wavelength 365 nm) with a photomask, and then sequentially baked again using hotplates at two different temperatures of 65 °C and 95 °C to crosslink the UV exposed parts of photoresist. The photoresist film was developed using propylene glycol monomethyl ether acetate (Aldrich) and rinsed with isopropyl alcohol (Merck). The patterned master was hard baked at 180 °C for 10 min on the hotplate, and then treated with chlorotrimethylsilane (Sigma-Aldrich) to prevent the adhesion between the master pattern and PDMS. The master pattern was molded by a soft-lithographic procedure using PDMS (PDMS 184-A and B, Dow Corning) for fabrication of microfluidic chips. PDMS 184-A (prepolymer) and 184-B (crosslinker) were mixed with a ratio of 10 : 1 and poured on the master pattern. The PDMS was cured on the master pattern at 70 °C for 2 h in a convection oven. The cured PDMS channel was then cut out and the coupler for optical fiber insertion, which was situated at the 'T' intersection of microfluidic channel, was opened using a razor blade. The PDMS channel was then bonded to a 2 mm thick flat layer of PDMS after oxygen plasma treatment of the surfaces to be bonded. Because the PDMS was not sufficiently rigid to support the mechanical stresses generated during device operation, the flat PDMS side was bonded to a glass substrate using oxygen plasma treatment. To ensure that the ethylene glycol remained in the core region, the PDMS chips were treated with (heptadecafluoro-1, 1, 2, 2-tetrahydrodecyl) trichlorosilane (FDTS, Gelest) to reduce the affinity of ethylene glycol for the PDMS microchannel.

2.2 Experimental procedures and characterizations

A liquid core with high refractive index was introduced into the microchannel using a syringe pump (KDS 200, KD Scientific). The liquid core of the waveguide consisted of a mixture of ethylene glycol ($n_{EG} = 1.432$) and a fluorescent dye. Ethylene glycol was selected as the core fluid because it is a good solvent for various dyes, and has a refractive index higher than that of PDMS ($n_{PDMS} = 1.406$).[22,23] As the fluorescent light source in the integrated optofluidic LA waveguide, three different dyes—rhodamine 6G ($\lambda_{max} = 596$ nm), fluorescein sodium salt ($\lambda_{max} = 557$ nm), and coumarine 1 ($\lambda_{max} = 464$ nm)—were dissolved respectively in the ethylene glycol at a concentration of 1 mM. The air cladding flow was driven by vacuum suction connected to the outlet of the channel.[29,30] The vacuum pressure was controlled in the range of 400–600 mmHg using a vacuum gauge and needle valve. The flow patterns of the liquid core were observed using an inverted optical microscope (Eclipse TE 2000-U, Nikon). The dye-containing liquid core was guided by the confining air cladding, as shown in Fig. 2a and b. The fluorescent dye molecules dissolved in the liquid core were excited using a 100 W mercury lamp (C-SHG1, Nikon) connected to an inverted optical microscope with a 0.3 NA objective lens (×10). The pumping spot size was about 2 mm in diameter and the optical power was about 15 mW. When the waveguide geometry is considered, we find that out of the 2 mm-diameter pumping spot, only the top surface of the waveguide (0.1 mm × 2 mm) could be used to absorb the light from the mercury lamp if the width of the core stream was an order of 100 μm. Therefore, the actual effective pumping power was about 1 mW. In Fig. 2c and d, the micrograph images display the fluorescent lights emitted from fluorescein sodium salt at two different pumping spots. The fluorescent light was captured and guided in the core solution due to the high refractive index contrast between the ethylene glycol core ($n_{EG} = 1.432$) and the air cladding ($n_{air} = 1.000$).

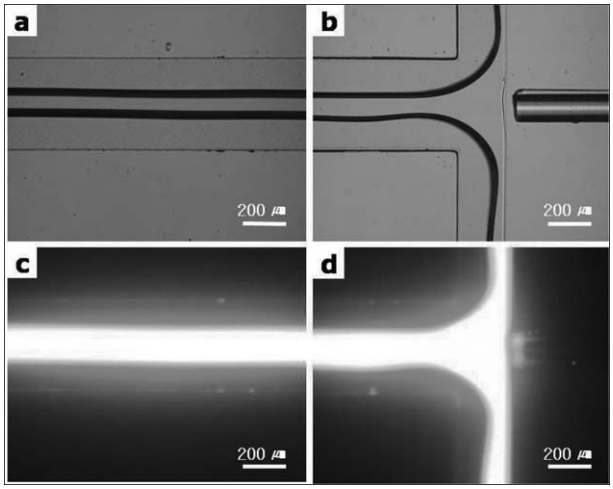

Fig. 2 (a, b) Optical micrographs and (c, d) fluorescent micrographs of two-phase stratified flows of ethylene glycol with fluorescein sodium salt and air for a LA waveguide operating with a core stream flow rate of 2 ml h^{-1} and a vacuum pressure of 400 mmHg in a microchannel of 140 μm in height. The pumping was performed at the spots covering the entire regions on the micrographs to obtain Fig. 2c and d.

The stream of liquid core was divided into two branches at the 'T' intersection in the PDMS microchannel, as shown in Fig. 2b and d. At the 'T' intersection of the core stream, the guided fluorescent light escaped from the core stream and coupled to the pre-aligned multimode optical fiber (step-index fiber, numerical aperture = 0.22, core diameter d_{core} = 105 μm, outer diameter d_{outer} = 125 μm), which was connected to an optical spectrometer (OSM-100-UV-NIR, Newport). The other side of the multimode optical fiber was cut using a fiber cleaver (FK11-4, PK Technology). The propagation loss was determined, using the microfluidic device shown in Fig. 1a, by measuring the optical power emitted from the waveguide as a function of the separation distance between the pumping spot and the 'T' intersection. The total coupling loss was calculated, using the microfluidic device shown in Fig. 1b, by coupling a known amount of optical power from a fiber pigtailed laser diode (LPM-635-SMA, Thorlabs). The optical power of the laser diode was controlled using a laser diode controller (LDC 205C, Thorlabs).

3. Results and discussion

In our system, three different dimensionless numbers, namely, capillary number Ca_L ($=\mu_L U_L/\gamma$), Bond number Bo_L ($=\rho_L g h^2/\gamma$), and Reynolds number Re_L ($=\rho_L U_L h/\mu_L$) characterize physics of flows and interfacial behavior by comparing a variety of relative effects involving surface tension, viscous force, gravitational force, and inertial force. Here, μ_L, ρ_L, g, and γ denote the viscosity and density of the liquid, gravitational acceleration, and surface tension, respectively. U_L represents the average velocity of the liquid flow and can be determined by dividing the volumetric liquid flow rate by the cross-sectional area of the liquid core stream. It should be noted that gravitational effects can be neglected when the Bond number, which is expressed as a ratio of gravitational force to surface tension, is very small. In our system, the Bond number (Bo_L) is estimated to be $4.52 \times 10^{-3} << 1$. The capillary number (Ca_L), which is expressed as a ratio of viscous force to surface tension, is found to be about $2.0 \times 10^{-2} << 1$. Therefore, one can safely assume that the air–liquid interface remains undeformed and provides optically smooth interface, and that the effects of the gravitational and viscous forces on the flow are negligible compared to the effect of surface tension. In addition, the Reynolds number (Re_L), which is expressed as a ratio of inertial to viscous forces, is found to be about 6.0×10^{-1}. Therefore, the stratified flow is in the laminar flow regime.

Huh *et al.* investigated the variations in flow behavior in systems with different surface affinities between water and PDMS microchannel wall in two-phase microfluidic systems having predominant surface tension effects.[29] Their result showed that the stable stratified flow of water and air could be achieved only when water has low affinity to the microchannel. Therefore, the hydrophobic treatment is essential to achieve the stable stratified flow of liquid and air. When assembling the microfluidic chip for the present LA waveguides, the top PDMS microchannel and bottom flat PDMS substrate were subjected to oxygen plasma treatment and then bonded to ensure complete sealing. When the ethylene glycol was dropped on the oxygen plasma treated flat PDMS substrate, complete wetting occurred due to its high affinity with the surface. Therefore, the fabricated PDMS microfluidic chips were treated with FDTS to reduce their affinity. After the FDTS treatment, the contact angle of ethylene glycol measured by the sessile drop method was 104°. Because of the irreversible chemical bonding between PDMS and FDTS, the surface property was not changed significantly for several months. A stable two-phase stratified flow of air and ethylene glycol could be achieved using the FDTS treated hydrophobic channel, as shown in Fig. 2.

Also, optically smooth side walls could be achieved in the two-phase stratified flow of LA waveguides due to the large surface tension between air and ethylene glycol and the low affinity between ethylene glycol and the FDTS-treated PDMS channel. In the LA waveguide developed in the present work, the large refractive index contrast between the core and the cladding ($\Delta n = n_{core} - n_{cladding}$) is expected to enhance the captured fraction. Assuming that a point light source lying in the center of circular waveguide, the analytical solution of captured fraction can be expressed as $\eta = \Delta n/2n_{core}$.[22] In actual fluorescent waveguides, however, the light sources are randomly distributed over the whole cross-section of the waveguide. In addition, the core stream is in contact with two materials, PDMS (on the top and bottom surfaces) and cladding fluid (on the lateral interfaces), as depicted in the inset of Fig. 1. In our system, the air–liquid meniscus is convex in shape due to the large contact angle of ethylene glycol on the FDTS treated PDMS (θ_{cont} = 104°). The meniscus is a part of a circle and the radius of curvature is affected by the contact angle of the core fluid because the gravitational effect is negligible for small Bond numbers (see Fig. S4†). In this case, the analytical calculation of captured fraction (η) is nontrivial, and we used the Monte Carlo simulation.†Note that the height of the core stream (h = 140 μm) is determined by the height of the microfluidic channel, and both contact angle (θ_{cont}) and height of core (h) are fixed during the fabrication step. Therefore, the captured fraction can be varied only by changing the maximum width (w) of the core stream.

Now we consider the tuning characteristics afforded by varying the core stream size by changing the flow rate of the core liquid or the air suction pressure. The same PDMS microfluidic channel of height 140 μm and width 400 μm was used in this experiment. In Fig. 3, the maximum width w of the core liquid stream is plotted as a function of the liquid core flow rate. As noted, the maximum width of the liquid core stream increases from 65 μm to 330 μm as we increase the core flow rate from 2 ml h^{-1} to 10 ml h^{-1} under a constant air suction pressure of 600 mmHg. Here, we note that the core size can also be varied by changing the suction pressure, which controls the air flow rate. For example, under a constant core flow rate of 2 ml h^{-1}, the maximum width w of the core stream increases from 65 μm to 115 μm when the suction pressure is decreased from 600 mmHg to 400 mmHg. Such size flexibility cannot be achieved using a conventional waveguide with a solid core and/or solid cladding.

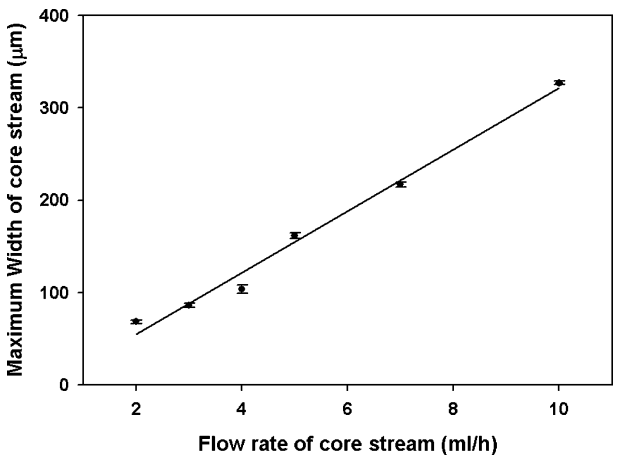

Fig. 3 The maximum width w of the liquid core stream as a function of the core stream flow rate at the fixed vacuum pressure of 600 mmHg. The width and height of the PDMS channel are fixed at 400 μm and 140 μm, respectively.

For the L^2 waveguide with water ($n_{water} = 1.331$) as the cladding layer and ethylene glycol ($n_{EG} = 1.432$) as the core fluid, η is in the range of 4.4–8.0% for 65 μm < w < 330 μm.[22] As mentioned above, diffusional mixing of the core and cladding liquids in this type of waveguide can reduce the refractive index contrast. This shortcoming could be remedied by employing immiscible fluids such as ethylene glycol and silicone oil ($n_{Si\ oil} = 1.401$);[22] however, this approach is usually accompanied by a further reduction of the refractive index contrast ($\Delta n = 0.031$), resulting in a low η (≈3%). In our LA waveguide with a liquid core and air cladding, by contrast, the larger refractive index contrast ($\Delta n = 0.432$) makes it possible to experimentally achieve captured fractions in the range of η = 9.9–22.8%, which are two- to three-fold greater than that of the L^2 counterpart. In addition, the LA waveguide is free from diffusional mixing.

To realize integrated optofluidic light sources, the fluorescent light should be efficiently guided in the core stream and then delivered to other optical components for actual applications. In the following discussion, we will focus on propagation loss in the LA waveguide, and compare it to propagation loss in the L^2 waveguide. For this purpose, we positioned an optical fiber connected to an optical spectrometer at the 'T' intersection of waveguide, as shown in Fig. 2b. The total coupling loss was calculated by coupling a known amount of optical power from a laser diode. The microfluidic device for the waveguide was slightly modified to couple the light from the laser diode (see Fig. 1b). The light from the laser diode was coupled to the 'T' intersection of the waveguide. The guided light from the waveguide was collected to the optical fiber inserted at the 'T' intersection on the opposite side. The measured total loss of the waveguide was 3.74 dB. The total coupling loss, which is calculated by subtracting the propagation loss of a 2 cm-long waveguide (0.84 dB), was 2.9 dB. Both optical fiber-to-waveguide and waveguide-to-optical fiber coupling losses were included in the total coupling loss.

The coupling and propagation losses were simultaneously measured as the total loss of the waveguide in a single measurement at a specific distance from the pumping spot. However, the coupling loss is omnipresent; therefore the coupling loss could not affect the intensity variation when the separation distance (d) between the pumping spot and the 'T' intersection was changed by using microfluidic devices with the configuration shown in Fig. 1a. The propagation loss could be accurately calculated from the normalized intensity variation when the distance d from the source was changed.

First, we investigated the behavior of LA waveguides with different emission wavelengths by using three distinct fluorescent dye molecules: rhodamine 6G (λ_{max} = 596 nm), fluorescein sodium salt (λ_{max} = 557 nm), and coumarine 1 (λ_{max} = 464 nm). Fig. 4 shows the normalized emission spectra obtained from the three LA waveguide systems. These spectra were recorded at d = 15 mm using a dye concentration of 1 mM. The maximum width of liquid core (w) for the fluorescent observation was maintained at 105 μm to match the core diameter of the optical fiber connected to the optical spectrometer. As we mentioned in the Experimental section, the actual effective pumping power was about 1 mW. Under the pumping power, the emitted optical power from the fluorescent LA waveguide was as high as 12 μW. The emitted power from the fluorescent LA waveguides is thus

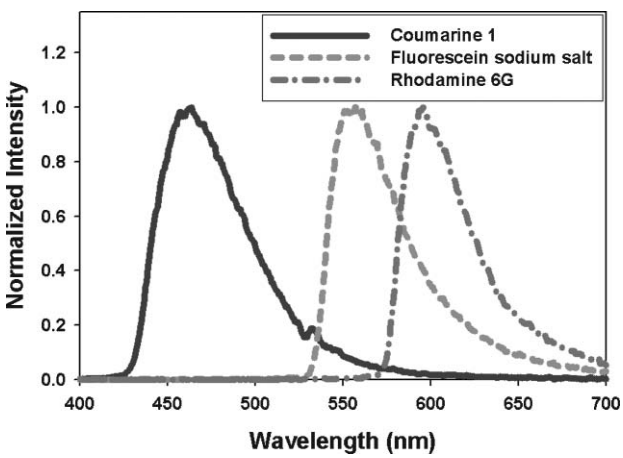

Fig. 4 Normalized emission spectra of LA waveguides with different dye molecules: rhodamine 6G (λ_{max} = 596 nm), fluorescein sodium salt (λ_{max} = 557 nm), and coumarine 1 (λ_{max} = 464 nm). In all experiments, the distance from the pumping spot and the dye concentration was fixed at 15 mm and 1 mM, respectively. The maximum width of the liquid core (w) for the fluorescent observation was 105 μm.

comparable to, or exceeds, the power of conventional fiber optic light sources for spectroscopy.[22] In addition, a specific wavelength of interest can be obtained simply by adding different dye molecules to the core fluid, because the core fluid (ethylene glycol) can dissolve a variety of dye molecules. Dye bleaching can be avoided by replenishing the dye molecules during operation of the LA waveguide.

Next we measured the emission spectra of the LA waveguide containing 1 mM rhodamine 6G at a range of separation distances (d) from the sources. Fig. 5a shows the fluorescent emission spectra for two different distances $d = 8$ and 15 mm from the pumping spot to the 'T' intersection. As expected, the spectral intensity decreases as the distance from source increases. However, this intensity drop is larger in the wavelength region of 570–600 nm. In the case of rhodamine 6G in ethylene glycol solution, the spectral overlap between absorption and emission is significant when the concentration exceeds 0.1 mM.[22] The more pronounced reduction in intensity can be explained by self-absorption of the guided light by the dye molecules in this wavelength region. Therefore, care must be taken to choose the proper wavelength region for accurate measurement of waveguide propagation losses.

We selected three representative wavelength regions: 590–600 nm, 610–620 nm, and 630–640 nm, designated as regions I, II and III (see Fig. 5a). Note that our LA waveguide should support numerous transverse optical modes (the V number of the waveguide is >180), due to its large refractive index difference (Δn) and large length scales (w, h) of the waveguide cross-section. In Fig. 5b, the average spectral intensity for each of the three wavelength regions is plotted as a function of the separation distance d in the range of $d = 8$–17 mm. In order to obtain reliable data of the waveguide propagation loss, we kept the separation distance d between the source and the 'T' intersection longer than 8 mm, considering the relatively large size (2 mm in diameter) of the effective pumping spot. If the pumping spot was closer than 8 mm, the pumping source excited fluorescent dye molecules around the branches of the 'T' intersection, which caused artifacts in the propagation loss. The estimated propagation losses are 0.64 dB cm^{-1}, 0.43 dB cm^{-1}, and 0.42 dB cm^{-1} for the three selected wavelength regions, I, II, and III, respectively. The slightly larger propagation loss in region I can be explained by self-absorption by dye molecules. For the other two dye molecules, fluorescein sodium salt (λ_{max} = 557 nm) and coumarine 1 (λ_{max} = 464 nm), the propagation losses were estimated by using the average spectral intensity at their respective region III (*i.e.*, 40 nm apart from the maximum emission wavelength) to minimize the self-absorption effect of dye molecules. The estimated propagation losses were 0.17 dB cm^{-1} and 0.14 dB cm^{-1}, respectively. The propagation losses for the LA waveguides are considerably small compared to those of other types of fluidic waveguides.[2,3,7,17,22,27]

Finally, we compared the propagation loss of the LA waveguide with that of the L^2 waveguide. Again, we compared the emission intensities in region III to minimize the self-absorption effect of dye molecules. For both types of waveguide, a 1 mM solution of rhodamine 6G in ethylene glycol (n_{EG} = 1.432) was introduced at a constant flow rate of 0.5 ml h^{-1}. For the LA waveguide, air (n_{air} = 1.000) flow was induced by 400 mmHg vacuum suction, while for the L^2 waveguide, water (n_{water} = 1.331) was introduced using a syringe pump. In the latter case, the water flow rate was set to 1 ml h^{-1} to make the maximum width

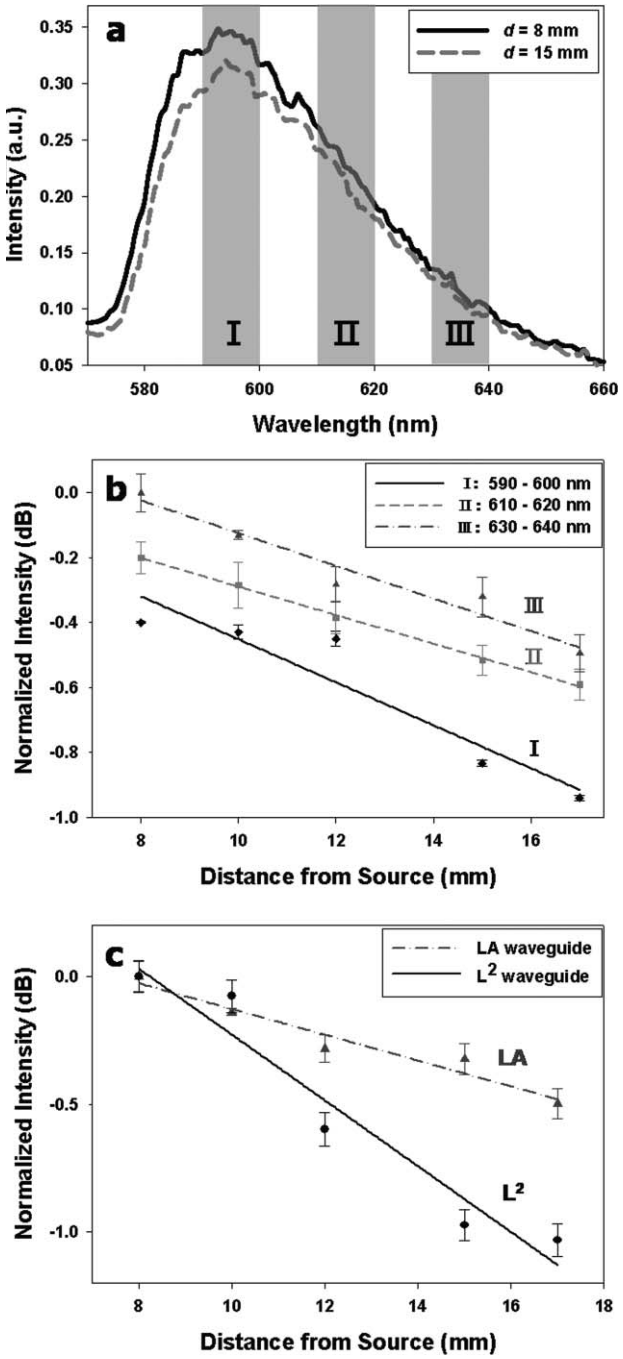

Fig. 5 (a) Emission spectra of a LA waveguide containing 1 mM rhodamine 6G at two different distances d of 8 and 15 mm from the source to the 'T' intersection. (b) The collected distinct fluorescent emission intensity as a function of the separation distance d for three selected wavelength regions: region I: 590–600 nm, region II: 610–620 nm, and region III: 630–640 nm. The estimated propagation losses are 0.64 dB cm^{-1}, 0.43 dB cm^{-1}, and 0.42 dB cm^{-1} for regions I, II, and III, respectively. The data points at regions I and II are shifted down by 0.4 dB and 0.2 dB, respectively, for clear distinction. (c) The average spectral intensity collected in region III as a function of the separation distance d. The core solution is introduced with a constant flow rate of 0.5 ml h^{-1}. Air (n_{air} = 1.000) and water (n_{water} = 1.331) are used as low refractive index cladding media for the LA and L^2 waveguides, respectively.

of the core stream for the L^2 waveguide similar with that of the LA waveguide. The average spectral intensity as a function of the distance d from the pumping spot is shown in Fig. 5c. The propagation loss of the LA waveguide was 0.42 dB cm^{-1}, whereas that of the L^2 waveguide was 1.32 dB cm^{-1}. The lower propagation loss of the LA waveguide arises mainly from its larger refractive index contrast.

Optical detection methods are widely used in micro-TAS. However, such methods require expensive and bulky components and precise alignment. The LA waveguide, by contrast, can be fabricated simply and inexpensively *via* PDMS based rapid prototyping. Because this fabrication method is compatible with the other parts of optofluidic devices, the fluorescent LA waveguide could be integrated into optofluidic devices with precise alignment. In addition, because the sheath fluid is air, it can be obtained from the environment. Therefore, space for sheath fluid storage is not required. Given that the sheath fluid occupies the most significant space for long term operation,[29] the LA waveguide may represent a more suitable option for portable light sources.

Conclusions

We developed the fluorescent LA waveguide for optofluidic light sources based on the two-phase stratified flow of ethylene glycol containing a fluorescent dye and air. The dye-containing ethylene glycol ($n_{EG} = 1.432$), which acts as a high refractive index core, is introduced into the microfluidic chip using a syringe pump with a controlled flow rate. Three different dye molecules—rhodamine 6G ($\lambda_{max} = 596$ nm), fluorescein sodium salt ($\lambda_{max} = 557$ nm), and coumarine 1 ($\lambda_{max} = 464$ nm)—were used to demonstrate the wavelength tunability of the fluorescent light sources. The flow of air ($n_{air} = 1.000$), which acts as a low refractive index cladding, is induced by vacuum suction. The size of the core stream could be tuned reversibly by changing the flow rate of ethylene glycol or the air suction pressure. Unlike the conventional L^2 waveguide, the LA waveguide is not affected by diffusional mixing. In addition, the LA waveguide has optically smooth side walls with strong optical confinement, enabling it to achieve captured fractions as high as 22.8% and propagation losses as low as 0.14 dB cm^{-1}. The fabrication method for the LA waveguide is based on the rapid prototyping of PDMS, which is inexpensive and widely used for the fabrication of microfluidic devices. Therefore, the fluorescent LA waveguide can be precisely aligned with other device components during the fabrication of actual integrated optofluidic devices. The fluorescent LA waveguides can be used as light sources for integrated optofluidic devices and micro-TAS.

Acknowledgements

This work was supported by a grant from the Creative Research Initiative Program of the MEST/KOSEF for 'Complementary Hybridization of Optical and Fluidic Devices for Integrated Optofluidic Systems'.

References

1 D. Psaltis, S. R. Quake and C. H. Yang, *Nature*, 2006, **442**, 381.
2 S. Balslev, A. M. Jorgensen, B. Bilenberg, K. B. Mogensen, D. Snakenborg, O. Geschke, J. P. Kutter and A. Kristensen, *Lab Chip*, 2006, **6**, 213.
3 P. Dress and H. Franke, *Appl. Phys. B: Lasers Opt.*, 1996, **63**, 12.
4 R. Manor, A. Datta, I. Ahmad, M. Holtz, S. Gangopadhyay and T. Dallas, *IEEE Sens. J.*, 2003, **3**, 687.
5 A. Datta, I. Y. Eom, A. Dhar, P. Kuban, R. Manor, I. Ahmad, S. Gangopadhyay, T. Dallas, M. Holtz, F. Temkin and P. K. Dasgupta, *IEEE Sens. J.*, 2003, **3**, 788.
6 V. J. Cadarso, C. Fernandez-Sanchez, A. Llobera, M. Darder and C. Dominguez, *Anal. Chem.*, 2008, **80**, 3498.
7 W. P. Risk, H. C. Kim, R. D. Miller, H. Temkin and S. Gangopadhyay, *Opt. Express*, 2004, **12**, 6446.
8 D. L. Yin, D. W. Deamer, H. Schmidt, J. P. Barber and A. R. Hawkins, *Opt. Lett.*, 2006, **31**, 2136.
9 D. L. Yin, E. J. Lunt, M. I. Rudenko, D. W. Deamer, A. R. Hawkins and H. Schmidt, *Lab Chip*, 2007, **7**, 1171.
10 P. Measor, L. Seballos, D. L. Yin, J. Z. Zhang, E. J. Lunt, A. R. Hawkins and H. Schmidt, *Appl. Phys. Lett.*, 2007, **90**, 211107.
11 D. Yin, E. J. Lunt, A. Barman, A. R. Hawkins and H. Schmidt, *Opt. Express*, 2007, **15**, 7290.
12 W. G. Yang, D. B. Conkey, B. Wu, D. L. Yin, A. R. Hawkins and H. Schmidt, *Nat. Photonics*, 2007, **1**, 331.
13 D. Erickson, T. Rockwood, T. Emery, A. Scherer and D. Psaltis, *Opt. Lett.*, 2006, **31**, 59.
14 T. T. Larsen, A. Bjarklev, D. S. Hermann and J. Broeng, *Opt. Express*, 2003, **11**, 2589.
15 C. J. S. de Matos, C. M. B. Cordeiro, E. M. dos Santos, J. S. K. Ong, A. Bozolan and C. H. B. Cruz, *Opt. Express*, 2007, **15**, 11207.
16 C. R. Rosberg, F. H. Bennet, D. N. Neshev, P. D. Rasmussen, O. Bang, W. Krolikowski, A. Bjarklev and Y. S. Kivshar, *Opt. Express*, 2007, **15**, 12145.
17 H. Y. Sun, F. He, Z. H. Zhou, Y. Cheng, Z. Z. Xu, K. Sugioka and K. Midorikawa, *Opt. Lett.*, 2007, **32**, 1536.
18 H. Schmidt and A. R. Hawkins, *Microfluid. Nanofluid.*, 2008, **4**, 3.
19 A. R. Hawkins and H. Schmidt, *Microfluid. Nanofluid.*, 2008, **4**, 17.
20 O. J. A. Schueller, X. M. Zhao, G. M. Whitesides, S. P. Smith and M. Prentiss, *Adv. Mater.*, 1999, **11**, 37.
21 D. B. Wolfe, R. S. Conroy, P. Garstecki, B. T. Mayers, M. A. Fischbach, K. E. Paul, M. Prentiss and G. M. Whitesides, *Proc. Natl. Acad. Sci. U. S. A.*, 2004, **101**, 12434.
22 D. V. Vezenov, B. T. Mayers, D. B. Wolfe and G. M. Whitesides, *Appl. Phys. Lett.*, 2005, **86**, 041104.
23 B. T. Mayers, D. V. Vezenov, V. I. Vullev and G. M. Whitesides, *Anal. Chem.*, 2005, **77**, 1310.
24 D. V. Vezenov, B. T. Mayers, R. S. Conroy, G. M. Whitesides, P. T. Snee, Y. Chan, D. G. Nocera and M. G. Bawendi, *J. Am. Chem. Soc.*, 2005, **127**, 8952.
25 D. B. Wolfe, D. V. Vezenov, B. T. Mayers, G. M. Whitesides, R. S. Conroy and M. G. Prentiss, *Appl. Phys. Lett.*, 2005, **87**, 181105.
26 M. Brown, T. Vestad, J. Oakey and D. W. M. Marr, *Appl. Phys. Lett.*, 2006, **88**, 134109.
27 C. L. Bliss, J. N. McMullin and C. J. Backhouse, *Lab Chip*, 2007, **7**, 1280.
28 C. L. Bliss, J. N. McMullin and C. J. Backhouse, *Lab Chip*, 2008, **8**, 143.
29 D. Huh, Y. C. Tung, H. H. Wei, J. B. Grotberg, S. J. Skerlos, K. Kurabayashi and S. Takayama, *Biomed. Microdevices*, 2002, **4**, 141.
30 D. Huh, A. H. Tkaczyk, J. H. Bahng, Y. Chang, H. H. Wei, J. B. Grotberg, C. J. Kim, K. Kurabayashi and S. Takayama, *J. Am. Chem. Soc.*, 2003, **125**, 14678.